Super-resolution Microscopy

International Edition: DOI: 10.1002/anie.201503215
German Edition: DOI: 10.1002/ange.201503215

SLAP: Small Labeling Pair for Single-Molecule Super-Resolution Imaging**

Ralph Wieneke, Anika Raulf, Alina Kollmannsperger, Mike Heilemann, and Robert Tampé**

Abstract: *Protein labeling with synthetic fluorescent probes is a key technology in chemical biology and biomedical research. A sensitive and efficient modular labeling approach (SLAP) was developed on the basis of a synthetic small-molecule recognition unit (Ni-trisNTA) and the genetically encoded minimal protein His_{6-10}-tag. High-density protein tracing by SLAP was demonstrated. This technique allows super-resolution fluorescence imaging and fulfills the necessary sampling criteria for single-molecule localization-based imaging techniques. It avoids masking by large probes, for example, antibodies, and supplies sensitive, precise, and robust size analysis of protein clusters (nanodomains).*

The target proximity achieved by small-molecule probes is essential to exploit the full potential of super-resolution fluorescence microscopy. Single-molecule localization techniques provide high spatial resolution by reporting on the position of the fluorophore and thus only indirectly on the target molecule itself.[1] Large labels, such as antibodies, can misleadingly position a fluorophore tens of nanometers away from the target.[2] Since single-molecule localization microscopy[3] can achieve almost the ultimate spatial precision (< 10 nm), large detection markers lead to mislocalization artifacts. The linkage error caused by displacement of the fluorophore not only limits the spatial resolution, but also impairs the quantitative analysis of single-molecule localization data. The gained signal-related information affects the accurate and robust determination of oligomeric states or cluster sizes of macromolecular complexes, as well as the determination of the relative target position.

Enhanced localization accuracy can be obtained with relatively large fusion proteins, such as SNAP-tag,[4] CLIP-tag,[5] Halo-tag,[6] DHFR-tag,[7] and smaller peptide motifs, for example, tetracysteine tags[8] or PRIME.[9] These approaches have one or more of the following drawbacks: 1) insufficient specificity, 2) compromised protein function, localization, or dynamics as a result of the steric constraints of the fusion domains, and 3) demand for the generation of new fusion constructs or the requirement for cofactors/enzymes for labeling. The ideal probe for single-molecule localization microscopy is small in size, allows stoichiometric labeling, operates with bright organic fluorophores, and permits high specificity. Efforts towards the introduction of such small labels include amber codon suppression and subsequent labeling through bioorthogonal chemistry.[10]

To achieve a labeling specificity comparable to antibodies, we developed the small labeling pair (SLAP) technology, which fulfills all of the necessary requirements for single-molecule localization microscopy. SLAP is based on a minimalistic lock-and-key element composed of the multivalent chelator head *tris*-*N*-nitrilotriacetic acid (Ni-*tris*NTA) and a minimal genetically encoded peptide tag (His_{6-10} tag). As a result of multivalency, Ni-*tris*NTA shows nanomolar affinity for His_6-tagged proteins ($K_D = 10$ nM), whereas the affinity for His_{10}-tagged proteins is in the subnanomolar range ($K_D = 0.1$ nM).[11] Furthermore, kinetically stable binding of Ni-*tris*NTA to an oligohistidine sequence ($k_{off} = 0.18\ h^{-1}$) allows long-term observation while maintaining reversibility in the presence of imidazole, histidine, and ethylenediaminetetraacetic acid (EDTA) for fluorophore exchange after photo-

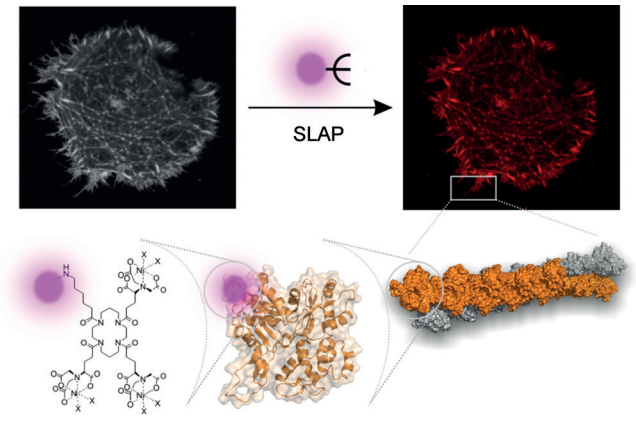

Figure 1. Site-specific targeting of His_{6-10}-tagged proteins with fluorescent Ni-*tris*NTA probes for super-resolution microscopy. Human cells transfected with His_{10}-^{eGFP}actin were chemically arrested, permeabilized, labeled with Ni-*tris*$NTA^{AlexaFluor647}$, and analyzed by confocal laser-scanning microscopy (CLSM). The image on the right demonstrates co-localization and site-specific labeling of His_{10}-tagged actin by the minimal lock-and-key element (Figure S1). Lower part: schematic illustration of the Ni-*tris*NTA/His-tag interaction on actin filaments.

[*] Dr. R. Wieneke,[+] A. Kollmannsperger, Prof. R. Tampé
Institute of Biochemistry, Biocenter; Cluster of Excellence Frankfurt
Goethe-University Frankfurt
Max-von-Laue-Str. 9, 60438 Frankfurt/M. (Germany)
E-mail: tampe@em.uni-frankfurt.de
Homepage: http://www.biochem.uni-frankfurt.de
http://www.smb.uni-frankfurt.de
A. Raulf,[+] Prof. M. Heilemann
Institute of Physical and Theoretical Chemistry
Goethe-University Frankfurt
Max-von-Laue-Str. 7, 60438 Frankfurt/M. (Germany)
E-mail: heilemann@chemie.uni-frankfurt.de
[+] These authors contributed equally to this work.

[**] This work was supported by the DFG (SPP 1623 and GRK 1986) to R.T. and the Cluster of Excellence Macromolecular Complexes.
Supporting information for this article is available on the WWW under http://dx.doi.org/10.1002/anie.201503215.

bleaching.[12] Recently, the targeting of His-tagged proteins in living cells has been realized through the carrier-mediated delivery of Ni-*tris*NTA, thus underscoring the unique specificity of Ni-*tris*NTA in the crowded environment of the cytosol.[13] Organic probes feature small size, superior quantum yield, photostability, and a broad range of emission spectra. Hence, conjugation to Ni-*tris*NTA would allow these benefits to be exploited. Co-localization with minimal linkage error can be achieved through the site-specific Ni-*tris*NTA/His-tag recognition because of the small size of the two interaction partners (< 1 nm; Figure 1). This promotes the facile labeling of proteins of interest with virtually any reporter dye. Herein, we demonstrate that SLAP enables the rapid, site-specific, and stoichiometric labeling of His-tagged proteins at various subcellular localizations for single-molecule localization-based imaging techniques.

In this study, we employed His_{10}-tagged variants of the cytoskeletal protein β-actin and the nuclear envelope protein laminA. For initial co-localization studies, we N-terminally fused the targets to an enhanced green fluorescent protein (eGFP). Human cervical cancer cells (HeLa) expressing His_{10}-^{eGFP}actin and Chinese hamster ovary (CHO-K1) cells expressing His_{10}-^{eGFP}laminA were chemically fixed and labeled with only 100 nM of Ni-*tris*NTA^{AlexaFluor647} for the specific targeting of His-tagged proteins. Confocal laser-scanning microscopy (CLSM) confirmed the accurate localization of the investigated proteins, together with a precise superposition with the reporter molecule Ni-*tris*NTA (Figures S1, S2 in the Supporting Information). Notably, nearly complete co-localization between the His_{10}-tagged protein and the small probe Ni-*tris*NTA was observed (Pearson coefficients: actin 0.85 ± 0.04; laminA 0.90 ± 0.05), thus confirming highly specific and stoichiometric staining. Specific labeling through SLAP was demonstrated in cells expressing a His-tag-deficient protein, as well as in non-transfected HeLa cells, in which neither co-localization nor unspecific background staining was observed (Figures S3, S4). The formation of the lock-and-key recognition pair is essential for sensitive detection, since nickel-free *tris*NTA^{AlexaFluor647} failed to label His-tagged proteins (Figure S5). In this case, unspecific binding events with AlexaFluor647-conjugated *tris*NTA were not detected. Moreover, reversibility and simple exchange of dye-labeled Ni-*tris*NTA were readily accomplished through treatment with EDTA or imidazole followed by further targeting through SLAP (Figures S6, S7). This is hardly achievable through immunofluorescence or covalent dye attachment (e.g., SNAP-tag). This modularity and high rate of labeling offers rapid iterative targeting of proteins for fluorescence microscopy, free choice of the reporter group, and sequential tracking.

Intrigued by these observations, we applied single-molecule localization microscopy[1e] and recorded fluorescence images of His_{10}-^{eGFP}actin with subdiffraction spatial resolution of the target protein (Figure 2 and Figures S8, S9). While reversibly photoswitching AlexaFluor647,[14] 20000 to 40000 images at a frame rate of 33 Hz were recorded. The reconstructed *d*STORM images enabled visualization of the filamentous structure of actin (Figure 2b) with subdiffraction spatial resolution and widths down to 40 nm for single actin filaments (Figure 2c). A similar procedure was applied to laminA and revealed high spatial resolution for laminA at the nuclear envelope (width down to 50 nm; Figure 2e) and for a traversing intranuclear cross-section of this filamentous protein (Figure 2f). Next to visual inspection of the spatial resolution, the localization precision was determined to be 16.6 ± 0.3 nm for actin and 14.5 ± 0.7 nm for laminA (Figure S10a, b) by using a nearest-neighbor distance analysis.[15] In comparison with the wide-field images (Figure 2a, d), a significant improvement in spatial resolution was obtained with our SLAP approach under *d*STORM conditions. This underscores the applicability and high target specificity of our minimalistic Ni-*tris*NTA/His-tag recognition pair for the close-proximity linkage of fluorophores to His-tagged targets.

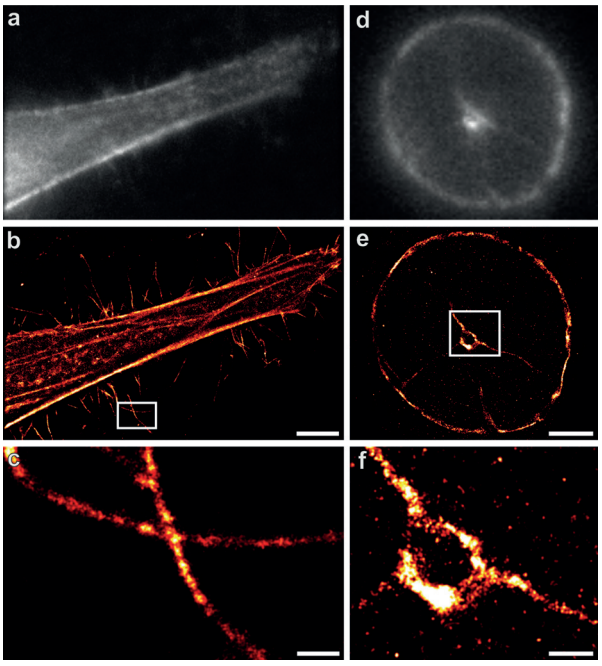

Figure 2. Single-molecule super-resolution microscopy of His_{10}-tagged proteins by using SLAP. HeLa cells transfected with His_{10}-^{eGFP}actin (a–c) and CHO-K1 cells transfected with His_{10}-^{eGFP}laminA (d–f) were chemically arrested, permeabilized, and labeled with Ni-*tris*NTA^{AlexaFluor647} (100 nM) through site-specific His_{10}-tag recognition. Reconstructed *d*STORM images of actin (b; scale bar 5 μm) and laminA (e; scale bar 2.5 μm) exhibit higher optical resolution than conventional fluorescence images (a, d). Magnifications of particular areas (c, f; scale bar 0.5 μm) illustrate the high-density labeling and superior resolution obtained by using SLAP.

We next evaluated the utility of SLAP for the analysis of macromolecular complexes. Single-molecule localization microscopy provides information on the size of protein clusters; however, this is often impaired by the large size of antibodies. By contrast, SLAP features stoichiometric labeling and, at the same, time close-proximity to the protein complex. The fluorescence-signal-related information from super-resolution images is hence directly associated with the cluster size, unperturbed by multiple or distantly located reporter probes. To demonstrate this, we utilized a His_{10}-tagged membrane-embedded subunit of the antigen translocation complex TAP. The transporter associated with antigen processing (TAP)

belongs to the ATP-binding cassette superfamily and resides in the endoplasmic reticulum (ER) membrane. As part of the adaptive immune response, TAP delivers proteasomal degradation products to the ER for the loading of major histocompatibility complex class I (MHC I) molecules as a primary defense strategy against infected and malignantly transformed cells.[16] The TAP complex is known to form higher-order clusters, but it had so far not been investigated with single-molecule imaging methods.[17]

We subjected HeLa cells transfected with TAP^{mVenus}-His_{10} to super-resolution microscopy with AlexaFluor647 by using either SLAP or conventional immunofluorescence (Figure 3; for comparison see CLSM images in Figure S11). To compare His_{10}-tag-specific targeting, a monoclonal anti-His antibody was used and the secondary antibody was coupled to AlexaFluor647 for readout (Figure S12). Upon excitation at 643 nm, 20000 to 40000 images were recorded in both approaches and reconstructed to obtain the *d*STORM images. Analysis of specific regions of TAP in the ER membrane with single-molecule sensitivity revealed structural details that had so far been hidden from conventional fluorescence microscopy. In both cases, nanometer-sized and clearly distinct clusters of TAP were observed (Figure 3a,c; see Figure S13). To determine the size of these clusters, we applied Ripley's H-function, which has been employed to analyze the surface clustering of the adaptor protein Lat during T-cell receptor (TCR) signaling.[18] The inputs for Ripley's H-function are the coordinates of single objects. For objects that are distributed uniformly in space, the H-function is zero at all length scales; positive values report locally clustered objects. Applied to single-molecule localization microscopy data, the coordinates of single fluorophores associated with the linked biomolecule serve as input parameters for the H-function. Hence, the H-function provides detailed information on the apparent target cluster size.

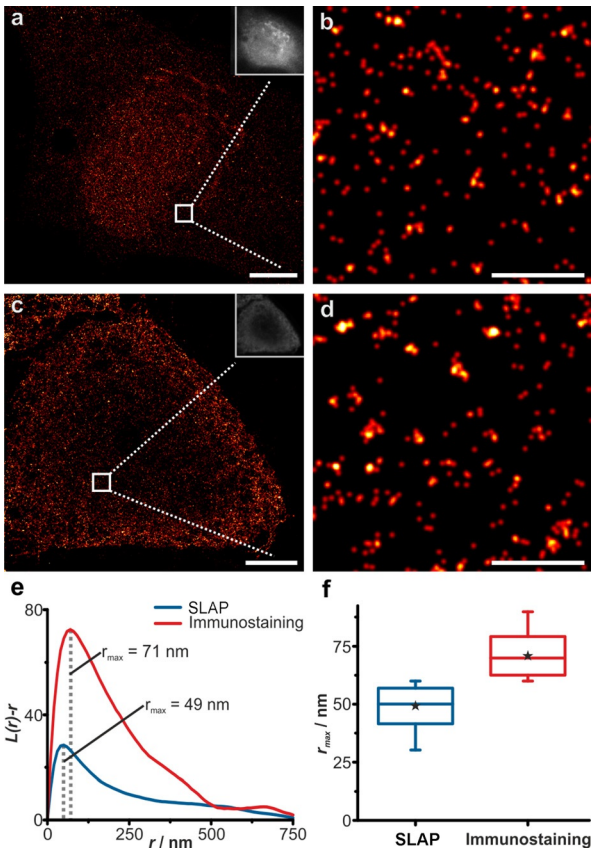

Figure 3. Super-resolution microscopy and suborganelle cluster analysis of TAP^{mVenus}-His_{10}. Transiently transfected HeLa cells were chemically arrested and permeabilized prior to labeling with Ni-*tris*-$NTA^{AlexaFluor647}$ (a, b) or through immunofluorescence (c, d). *d*STORM images show TAP^{mVenus}-His_{10} located in the ER membrane (a, c; scale bar: 5 μm). 1.5 μm^2 regions (b, d) were analyzed by using Ripley's H-function (e) to yield the apparent cluster sizes (f). The average cluster size of Ni-*tris*NTA-stained TAP^{mVenus}-His_{10} (49 ± 7 nm) is significantly smaller than the antibody-stained TAP (71 ± 8 nm).

By calculating Ripley's H-function for TAP marked by SLAP, an average cluster size of 49 ± 7 nm was determined. By contrast, the cluster dimension for immunostained TAP was assigned as 71 ± 8 nm. The latter value is significantly enlarged by the extended size of the antibodies as well as by the fact that two antibodies were used. The radius difference of 22 nm is in excellent agreement with the radius increment calculated for two antibodies (2×10 nm). Moreover, the cluster size is significantly larger than the localization precision (Figure S10c,d), thus implying that TAP assembles into higher-order oligomers (nanoclusters) within the ER membrane, an unprecedented result for TAP at the single-molecule level. It is important to note that no significant difference in the localization precision of SLAP-labeled TAP^{mVenus}-His_{10} (12.3 ± 0.3 nm) compared to immunostained TAP^{mVenus}-His_{10} (11.9 ± 0.3 nm) was detected (Figure S10c,d). The size of TAP in nanoclusters is comparable to that of other macromolecular complexes measured at high spatial precision, for example, glycosylphosphatidylinositol-anchored CD59 (GPI-anchored CD59, ≥ 48 nm).[19]

Since the peptide-loading complex is composed of TAP, tapasin, calreticulin, ERp57, and MHC I molecules,[20] our data indicate an additional level of complexity for their organization into nanodomains or "protein islands". The preassembly of macromolecular complexes into "protein islands" might be important for their function, since this restricts diffusion in the ER membrane and is advantageous for a fast cooperative cellular response by the peptide-loading complex, which is in agreement with earlier observations from FRAP experiments.[17a] So far, conventional microscopy and immunostaining have not provided detailed information for an accurate and quantitative investigation of the observed nanoclusters. Stoichiometric targeting and high-density labeling with SLAP, in combination with single-molecule localization microscopy, revealed hidden structural details with near-molecular resolution. These details remained unresolved during ensemble measurements by conventional CLSM. In order to exactly determine the copy numbers and absolute stoichiometry of TAP within the nanodomains, photoactivatable fluorophores that do not exhibit reversible photoswitching are required. This avoids artefacts from over-counting because of multiple blinking cycles. In this study, the bright and best-performing photoswitchable fluorophore AlexaFluor647 was applied to demonstrate subdiffractional single-molecule localization microscopy. We are currently develop-

ing caged fluorophores that do not exhibit photoswitching upon light activation for quantification purposes.

In summary, we introduce SLAP as a small-molecule detection pair for super-resolution microscopy of target structures. The high specificity, high-density, and stoichiometric labeling of distinct His_{6-10}-tagged proteins was achieved with excellent signal-to-noise and signal-to-background ratios. The close proximity of the Ni-*tris*NTA/His_{6-10}-tag recognition pair accounts for the high spatial resolution and highlights the utility of small detection probes for significantly enhancing resolution. Bioorthogonal labeling approaches with other small-molecule probes would help decipher complex cellular processes, transient protein–protein interactions, or early events in signal transduction, for example, receptor clustering. Currently, we are developing spatiotemporal targeting of His_{6-10}-tagged proteins for single-molecule tracking and localization analysis in live intact cells, based on our recently established photoactivatable Ni-*tris*NTA (PA-*tris*NTA).[21] Virtually every functional His-tagged construct could be subjected to single-molecule localization studies facilitated by SLAP with minimal effort and time investment. Our efficient and modular technique will thus pave the way to high-throughput localization analysis of almost the entire His-tagged proteome, whenever possible, at ultimate spatial resolution.

Keywords: bioorthogonal chemistry · chemical biology · proteins · single-molecule imaging · super-resolution microscopy

How to cite: *Angew. Chem. Int. Ed.* **2015**, *54*, 10216–10219
Angew. Chem. **2015**, *127*, 10354–10357

[1] a) M. Sauer, *J. Cell Sci.* **2013**, *126*, 3505–3513; b) S. W. Hell, *Science* **2007**, *316*, 1153–1158; c) E. Betzig, G. H. Patterson, R. Sougrat, O. W. Lindwasser, S. Olenych, J. S. Bonifacino, M. W. Davidson, J. Lippincott-Schwartz, H. F. Hess, *Science* **2006**, *313*, 1642–1645; d) M. J. Rust, M. Bates, X. Zhuang, *Nat. Methods* **2006**, *3*, 793–795; e) M. Heilemann, S. van de Linde, M. Schuttpelz, R. Kasper, B. Seefeldt, A. Mukherjee, P. Tinnefeld, M. Sauer, *Angew. Chem. Int. Ed.* **2008**, *47*, 6172–6176; *Angew. Chem.* **2008**, *120*, 6266–6271; f) M. Heilemann, S. van de Linde, A. Mukherjee, M. Sauer, *Angew. Chem. Int. Ed.* **2009**, *48*, 6903–6908; *Angew. Chem.* **2009**, *121*, 7036–7041.

[2] J. Ries, C. Kaplan, E. Platonova, H. Eghlidi, H. Ewers, *Nat. Methods* **2012**, *9*, 582–584.

[3] A. Fürstenberg, M. Heilemann, *Phys. Chem. Chem. Phys.* **2013**, *15*, 14919–14930.

[4] a) A. Keppler, S. Gendreizig, T. Gronemeyer, H. Pick, H. Vogel, K. Johnsson, *Nat. Biotechnol.* **2002**, *21*, 86–89; b) A. Keppler, H. Pick, C. Arrivoli, H. Vogel, K. Johnsson, *Proc. Natl. Acad. Sci. USA* **2003**, *101*, 9955–9959.

[5] A. Gautier, A. Juillerat, C. Heinis, I. R. Correa, Jr., M. Kindermann, F. Beaufils, K. Johnsson, *Chem. Biol.* **2008**, *15*, 128–136.

[6] G. V. Los, L. P. Encell, M. G. McDougall, D. D. Hartzell, N. Karassina, C. Zimprich, M. G. Wood, R. Learish, R. F. Ohana, M. Urh, D. Simpson, J. Mendez, K. Zimmerman, P. Otto, G. Vidugiris, J. Zhu, A. Darzins, D. H. Klaubert, R. F. Bulleit, K. V. Wood, *ACS Chem. Biol.* **2008**, *3*, 373–382.

[7] C. Jing, V. W. Cornish, *ACS Chem. Biol.* **2013**, *8*, 1704–1712.

[8] a) B. A. Griffin, S. R. Adams, R. Y. Tsien, *Science* **1998**, *281*, 269–272; b) S. R. Adams, R. E. Campbell, L. A. Gross, B. R. Martin, G. K. Walkup, Y. Yao, J. Llopis, R. Y. Tsien, *J. Am. Chem. Soc.* **2002**, *124*, 6063–6076.

[9] a) C. Uttamapinant, K. A. White, H. Baruah, S. Thompson, M. Fernandez-Suarez, S. Puthenveetil, A. Y. Ting, *Proc. Natl. Acad. Sci. USA* **2010**, *107*, 10914–10919; b) C. Uttamapinant, A. Tangpeerachaikul, S. Grecian, S. Clarke, U. Singh, P. Slade, K. R. Gee, A. Y. Ting, *Angew. Chem. Int. Ed.* **2012**, *51*, 5852–5856; *Angew. Chem.* **2012**, *124*, 5954–5958.

[10] a) T. Plass, S. Milles, C. Koehler, C. Schultz, E. A. Lemke, *Angew. Chem. Int. Ed.* **2011**, *50*, 3878–3881; *Angew. Chem.* **2011**, *123*, 3964–3967; b) K. Lang, L. Davis, J. Torres-Kolbus, C. Chou, A. Deiters, J. W. Chin, *Nat. Chem.* **2012**, *4*, 298–304; c) T. Plass, S. Milles, C. Koehler, J. Szymanski, R. Mueller, M. Wiessler, C. Schultz, E. A. Lemke, *Angew. Chem. Int. Ed.* **2012**, *51*, 4166–4170; *Angew. Chem.* **2012**, *124*, 4242–4246; d) K. Lang, L. Davis, S. Wallace, M. Mahesh, D. J. Cox, M. L. Blackman, J. M. Fox, J. W. Chin, *J. Am. Chem. Soc.* **2012**, *134*, 10317–10320; e) I. Nikić, T. Plass, O. Schraidt, J. Szymański, J. A. Briggs, C. Schultz, E. A. Lemke, *Angew. Chem. Int. Ed.* **2014**, *53*, 2245–2249; *Angew. Chem.* **2014**, *126*, 2278–2282.

[11] S. Lata, A. Reichel, R. Brock, R. Tampé, J. Piehler, *J. Am. Chem. Soc.* **2005**, *127*, 10205–10215.

[12] G. Giannone, E. Hosy, F. Levet, A. Constals, K. Schulze, A. I. Sobolevsky, M. P. Rosconi, E. Gouaux, R. Tampé, D. Choquet, L. Cognet, *Biophys. J.* **2010**, *99*, 1303–1310.

[13] R. Wieneke, N. Labòria, M. Rajan, A. Kollmannsperger, F. Natale, M. C. Cardoso, R. Tampé, *J. Am. Chem. Soc.* **2014**, *136*, 13975–13978.

[14] M. Heilemann, E. Margeat, R. Kasper, M. Sauer, P. Tinnefeld, *J. Am. Chem. Soc.* **2005**, *127*, 3801–3806.

[15] U. Endesfelder, S. Malkusch, F. Fricke, M. Heilemann, *Histochem. Cell Biol.* **2014**, *141*, 629–638.

[16] D. Parcej, R. Tampé, *Nat. Chem. Biol.* **2010**, *6*, 572–580.

[17] a) E. A. Reits, J. C. Vos, M. Gromme, J. Neefjes, *Nature* **2000**, *404*, 774–778; b) D. Marguet, E. T. Spiliotis, T. Pentcheva, M. Lebowitz, J. Schneck, M. Edidin, *Immunity* **1999**, *11*, 231–240.

[18] a) B. D. Ripley, *J. R. Stat. Soc. Series B Stat. Methodol.* **1977**, *39*, 172–192; b) B. F. Lillemeier, M. A. Mortelmaier, M. B. Forstner, J. B. Huppa, J. T. Groves, M. M. Davis, *Nat. Immunol.* **2010**, *11*, 90–96; c) D. J. Williamson, D. M. Owen, J. Rossy, A. Magenau, M. Wehrmann, J. J. Gooding, K. Gaus, *Nat. Immunol.* **2011**, *12*, 655–662.

[19] a) K. G. Suzuki, T. K. Fujiwara, M. Edidin, A. Kusumi, *J. Cell Biol.* **2007**, *177*, 731–742; b) K. G. Suzuki, T. K. Fujiwara, F. Sanematsu, R. Iino, M. Edidin, A. Kusumi, *J. Cell Biol.* **2007**, *177*, 717–730.

[20] S. Hulpke, R. Tampé, *Trends Biochem. Sci.* **2013**, *38*, 412–420.

[21] N. Labòria, R. Wieneke, R. Tampé, *Angew. Chem. Int. Ed.* **2013**, *52*, 848–853; *Angew. Chem.* **2013**, *125*, 880–886.

Received: April 8, 2015
Revised: May 23, 2015
Published online: July 14, 2015

